



1 **Channel flow, tectonic overpressure, and exhumation of** 2 **high-pressure rocks in the Greater Himalayas**

3 **Fernando O. Marques^{1*}, Nibir Mandal², Subhajit Ghosh³, Giorgio Ranalli⁴,**
 4 **Santanu Bose³**

5 *¹Universidade de Lisboa, Lisboa, Portugal*

6 *²Jadavpur University, Kolkata, India*

7 *³University of Calcutta, Kolkata, India*

8 *⁴Carleton University, Ottawa, Canada*

10 **Abstract**

11 The Himalayas are the archetype of continental collision, where a number of long-
 12 standing fundamental problems persist in the Greater Himalayan Sequence (GHS): (1)
 13 contemporaneous reverse and normal faulting; (2) inversion of metamorphic grade; (3) origin of
 14 high- (HP) and ultra-high (UHP) pressure rocks; (4) mode of ductile extrusion and exhumation
 15 of HP and UHP rocks close to the GHS hanging wall; (5) flow kinematics in the subduction
 16 channel; and (6) tectonic overpressure, here defined as $TOP = P/P_L$ where P is total (dynamic)
 17 pressure and P_L is lithostatic pressure. In this study we couple Himalayan geodynamics to
 18 numerical simulations to show how one single model, upward-tapering channel (UTC) flow, can
 19 be used to find a unified explanation for the evidence. The UTC simulates a flat-ramp geometry
 20 of the main underthrust faults, as proposed for many sections across the Himalayan continental
 21 subduction. Based on the current knowledge of the Himalayan subduction channel geometry and
 22 geological/geophysical data, the simulations predict that a UTC can be responsible for high TOP
 23 (> 2). TOP increases exponentially with decrease in UTC's mouth width, and with increase in
 24 underthrusting velocity and channel viscosity. The highest overpressure occurs at depths < -60



25 km, which, combined with the flow configuration in the UTC, forces HP and UHP rocks to
26 exhume along the channel's hanging wall, as in the Himalayas. By matching the computed
27 velocities and pressures with geological data, we constrain the GHS's viscosity to be $\leq 10^{21}$ Pa s,
28 and the effective convergence (transpression) to a value $\leq 10\%$. Variations in channel dip over
29 time ($>$ or $< 15^\circ$) may promote or inhibit exhumation, respectively. Viscous deformable walls do
30 not affect overpressure significantly for a viscosity contrast (viscosity walls/viscosity channel) in
31 the order of 1000 or 100. *TOP* in a UTC, however, is only possible if the condition at the bottom
32 boundary is no outlet pressure; otherwise it behaves as a leaking boundary that cannot retain
33 dynamic pressure. However, the cold, thick and strong lithospheres forming the Indian and
34 Eurasian plates are a good argument against a leaking bottom boundary in a flat-ramp geometry,
35 and therefore it is possible for overpressure to reach high values in the GHS.

36

37 Keywords: Himalayan geodynamics; channel flow; Greater Himalayas; numerical modelling;
38 tectonic overpressure; exhumation HP and UHP rocks

39

40 *Corresponding author. E-mail address: fomarques@fc.ul.pt

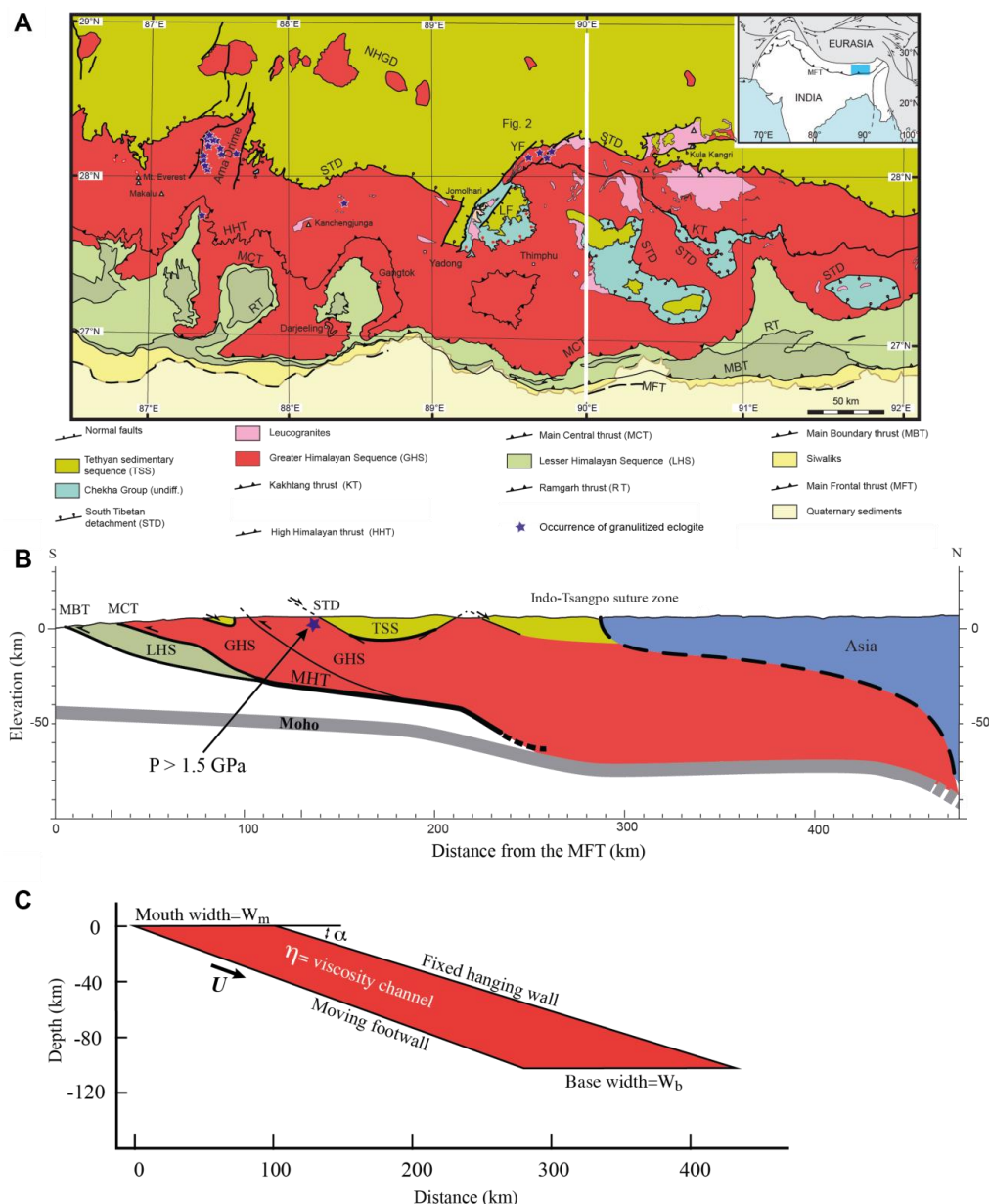
41

42 1. Introduction

43 Continental collision has brought together two continents, India and Eurasia, which were
44 previously separated by thousands of kilometres of oceanic lithosphere that has been consumed
45 by subduction. Understanding the mechanics of the collisional interface, known as the Greater
46 Himalayas Sequence (GHS), has continuously stimulated geoscientists to search for new
47 concepts/models. Most critically, high- (HP) and ultrahigh- (UHP) pressure rocks crop out along
48 the Himalayan GHS, thus raising long-standing and lively debated questions regarding formation
49 and exhumation of HP and UHP rocks, and the difference between lithostatic and dynamic



pressures (overpressure) in dynamic systems. The GHS appears therefore as a unique natural
prototype that can be modelled numerically in the search for answers to those critical questions.



52

53 *Figure 1. Geological setting of the eastern Himalayas, highlighting the architecture of its major tectonic*
 54 *elements. A – Simplified geological map of the eastern Himalayas (adapted from Grujic et al., 2011;*
 55 *Unsworth et al., 2005). White line along 90°E marks the cross-section shown in B. B – Schematic section*
 56 *across the Himalayas (adapted from Grujic et al., 2011), in which the UTC stands out (GHS in red). The*



57 *GHS is bounded at the top by the South Tibet Detachment (STD) and at the bottom by the Main Central*
58 *Thrust (MCT). MHT – Main Himalayan Thrust. C – Model setup of the UTC, with shape and dimensions*
59 *similar to the natural prototype in B. The “foot wall” (moving wall) and the “hanging wall” (no slip*
60 *wall) correspond to the MCT and the STD, respectively. Apart from the later folding of both MCT and*
61 *STD, the similarity between nature and model setup is apparent.*
62

63 1.1. Geological setting

64 Based on metamorphic grade and structural style, four units and the major faults
65 separating them were distinguished by Gansser (1964), which are from bottom to top (Fig. 1):
66 Sub-Himalayan Sequence (SHS – unmetamorphosed Tertiary rocks), Main Boundary Thrust
67 (MBT), Lesser Himalayan Sequence (LHS – low-grade metamorphic rocks), Main Central
68 Thrust (MCT), Greater Himalayan Sequence (GHS – high-grade metamorphic rocks), South
69 Tibetan Detachment (STD), and Tethyan Sedimentary Sequence (TSS – unmetamorphosed to
70 weakly metamorphosed rocks). All the main faults are N-dipping thrusts, except the STD that
71 also dips to N but is a normal fault.

72 The GHS shows patchy occurrences of eclogites close to the STD (Grujic et al., 2011;
73 Ganguly et al., 2000; O’Brien et al., 2001; Groppo et al., 2007; Corrie et al., 2010; Kellett et al.,
74 2013; Sorcar et al., 2014; Zhang et al., 2015) (Fig. 1A). Recent petrologic studies provide
75 estimates for spatial-temporal variations of pressure (P) and temperature (T) in the GHS. The
76 peak metamorphic conditions are $T \sim 760$ °C and $P \geq 1.5$ GPa for eclogitization in the Bhutan
77 Himalayas (Grujic et al., 2011). Peak conditions with $T = 670$ °C and $P \geq 1.5$ GPa were reported
78 for the Nepal Himalayas (Corrie et al., 2010). On the other hand, an estimate of the metamorphic
79 peak at $P = 2.7\text{--}2.9$ GPa and $T = 690\text{--}750$ °C from coesite-bearing eclogites in the western
80 Himalayas was provided by O’Brien et al. (2001). The eclogites have been in part overprinted by
81 regionally more extensive granulite facies conditions of 800 °C at ~ 1 GPa (Grujic et al., 2011;
82 Ganguly et al., 2000; Groppo et al., 2007; Zhang et al., 2015). PT -time paths suggest exhumation
83 of these high-grade rocks under nearly isothermal decompression after peak metamorphic
84 conditions (Ganguly et al., 2000; Groppo et al., 2007; Sorcar et al., 2014). Using cooling rates,



85 the exhumation history of the high-grade rocks was interpreted as a two-stage event by Ganguly
86 et al. (2000), marked by exhumation at a rate of 15 mm/yr to a depth of 15 km, followed by slow
87 exhumation at a rate of 2 mm/yr to a depth of at least 5 km, which occurred broadly in Miocene
88 times (Grujic et al., 2011; Corrie et al., 2010; Kellett et al., 2013; Sorcar et al., 2014; Warren et
89 al., 2011; Rubatto et al., 2013).

90 The exhumation mechanics of GHS rocks is one of the most debated issues in the
91 Himalayas (and elsewhere where HP and UHP rocks outcrop), having led to a variety of tectonic
92 models that postulate channel flow by topographic forcing (Wobus et al., 2005; Beaumont et al.,
93 2001) or transpression (Grujic et al., 1996). Grujic et al. (1996) first proposed the GHS in the
94 Bhutan Himalayas as deep crustal ductile rocks extruded between the MCT and the STD.
95 Numerical models have integrated geological, tectonic, geophysical, metamorphic and
96 rheological data to provide possible explanations for the exhumation process. The models
97 postulate a channel flow of low-viscosity rocks in the middle to lower crust, driven by
98 topographic pressure gradient, to account for the extrusion dynamics of high-grade metamorphic
99 rocks in the GHS (Wobus et al., 2005; Beaumont et al., 2001). The channel flow model can also
100 explain the coeval reverse and normal kinematics along the MCT and STD, respectively (Fig.
101 1B). However, as Grujic et al. (2011) pointed out, these models cannot “*predict the exhumation*
102 *of lower orogenic (>50 km, i.e. >1.4 GPa) crustal material*” in their basic form. To overcome
103 this limitation, an alternative exhumation mechanism was proposed by Grujic et al. (2011), with
104 additional tectonic forcing (transpression) by the impingement of strong Indian crust into the
105 already weak lower crustal granulitized eclogites below southern Tibet. However, previous
106 models do not comprehensively address the mechanics of overpressure leading to the formation
107 of eclogites (Schulte-Pelkum et al., 2005), and their focused exhumation close to the STD.

108 Given that the current models do not fully explain the observations in the GHS, in this
109 study we couple eastern Himalayan geodynamics with numerical simulations to show how one



single model, upward-tapering channel (UTC) flow, as in the current eastern Himalayas (Fig. 1B), can be used to find a unified explanation for the following persisting problems: (1) contemporaneous reverse and normal faulting; (2) inversion of metamorphic grade; (3) origin of high- (HP) and ultrahigh- (UHP) pressure rocks; (4) mode of ductile extrusion and exhumation of HP and UHP rocks close to the GHS hanging wall (STD); (5) flow kinematics in the subduction channel; and (6) tectonic overpressure.

116

1.2. Premises

We model channel flow with a linear viscous fluid by the Navier-Stokes equation with body force (gravity), therefore pressure in the channel depends on viscosity and velocity configuration. Most critically, the velocity field depends on channel geometry and conditions applied at the boundaries (e.g. Marques et al., 2018). Ultimately, *TOP* can only exist if the channel walls are strong enough. Therefore, when investigating pressure in a viscous channel, one has to take into account four fundamental issues:

(1) *Viscosity* – the viscosity term in the Navier-Stokes equation depends on a number of parameters, all of which are incorporated in the Arrhenius term in a constitutive equation. Therefore, the modeller has two options when investigating the effects of viscosity on pressure: either use a full constitutive equation and test all the parameters in the Arrhenius term, or simply and directly vary the magnitude of the viscosity. We chose the second option in our numerical simulations, since our focus is the assessment of parameter variations on the development of overpressure and flow configuration.

(2) *Geometry of the channel* – given that flow configuration inside the channel plays a critical role in the pressure distribution, we tested three main shapes of the channel: parallel-sided (parallelepiped), and upward (similarly to Marques et al., 2018) or downward tapering channels.



135 (3) *Boundary conditions* – the conditions at the boundaries can either promote or inhibit *TOP*,
136 because they control the flow pattern and the pressure retention inside the channel.
137 Therefore, we tested different velocity configurations applied at the underthrusting (foot)
138 wall (simple or simple+pure shears), and different conditions at the boundaries like slip, no-
139 slip or outlet pressure.

140 (4) *How the walls of the pressure vessel react to internal pressure* – under particular applied
141 boundary conditions, the Navier-Stokes equation produces *TOP* in an upward tapering
142 channel that can reach values orders of magnitude greater than observed in nature; therefore
143 we will discuss the theoretical values in view of the current knowledge on natural HP and
144 UHP rocks. The discussion of channel flow is similar to discussing a pressure vessel with an
145 overpressured fluid inside: one has to investigate the conditions to produce overpressure
146 inside the vessel (the channel in the prototype), and simultaneously the strength of the vessel
147 walls (the lithosphere in the prototype) to support the internal pressure without failure (by
148 brittle or viscous yield). We will therefore discuss the strength of the channel walls in view
149 of the current knowledge about the Indian (footwall) and Eurasian (hanging wall)
150 lithospheres, especially in terms of thickness and strength.

151

152 This study builds on the conceptual work by Marques et al. (2018) on tectonic
153 overpressure.

154 Given the above premises, we investigated the conditions under which overpressured
155 rocks can form and be exhumed in a prototype like the Himalayas: geometry of the channel,
156 conditions at the boundaries, applied velocities, and viscosity. Based on the numerical
157 simulations and the current knowledge of the Himalayas, we discuss the theoretical values of
158 overpressure, the obtained exhumation velocities, the most likely viscosity of the subducted
159 rocks, and finally the effects of the strength of the channel walls on overpressure.



160

161 **2. Numerical modelling**

162 We modelled the subduction channel, as illustrated in Fig. 1C, with an incompressible
 163 linearly viscous fluid, which has been accepted as a simple but effective approximation to the
 164 behaviour of rocks undergoing ductile flow. The setup simulates a flat-ramp geometry of the
 165 main underthrust faults, as shown in many cross-sections of the Himalayas, in particular the one
 166 shown in Fig. 1B. For steady-state flow of a viscous incompressible Newtonian fluid at very low
 167 Reynolds number, the dynamic Navier-Stokes equations reduce to the Stokes approximation,
 168 which is the basis of the COMSOL code for computational fluid dynamics used here.

169

170 *2.1. Boundary conditions and model setup*

171 The boundary conditions were as follows (see Fig. 1C, and Methods in Appendix for
 172 further details): (1) slab-parallel velocity (U) applied on the underthrusting (foot)wall (2 to 20
 173 cm/yr) (Feldl and Bilham, 2006; DeMets et al., 2010), and fixed hanging wall; (2) viscosity (η)
 174 between 10^{19} and 10^{22} Pa s (Beaumont et al., 2001; England and Houseman, 1989; Copley et al.,
 175 2011); (3) channel dip α (15 - 30°); (4) channel mouth's width $W_m = 25$ to 100 km, and width at
 176 the channel's base $W_b = 150$ or 200 km, from which we define $W_m^* = W_m/W_b$; (5) constant
 177 density of the material in the channel (2800 kg/m^3). Given the viscosity contrast between
 178 foot/hanging walls of the GHS and channel material, the channel walls were assumed
 179 undeformable in the first simulations, except when testing the effects of non-rigid walls on
 180 overpressure.

181 The metamorphic processes occur in response to the total isotropic stress, called *dynamic*
 182 *pressure*, which is a sum of the tectonic (Stokes) and lithostatic pressures ($\rho g z$, where ρ is
 183 density, g is gravitational acceleration, and z is depth). We evaluate the dynamic pressure to
 184 explain the occurrence of high-pressure rocks in the GHS, and we define an overpressure factor



185 (TOP) as the non-dimensional ratio between dynamic and lithostatic pressures (Figs. A1 and
 186 A2). For a better understanding of overpressure in a UTC, we carried out a parametric study of
 187 TOP as a function of η , W_m , α , U , and effective convergence velocity (transpression) (see
 188 Methods in Appendix for details). The prime focus of our investigation concerned the
 189 simulations with $U = 5$ cm/yr, $\alpha = 20^\circ$, $W_m = 100$ km and $W_b = 150$ km, which represent the most
 190 common and conservative values. We then use the numerical results to constrain the viscosity,
 191 pressure and velocity in the channel, consistent with current geological data and estimates.

192

193 **3. Model results**

194 *3.1. Flow patterns*

195 The model UTC shows two main layers, one flowing downward due to applied
 196 underthrusting motion in the footwall, and another flowing upward and so inducing relative
 197 normal faulting on the hanging wall (Fig. 2). Two distinct flow cells exist, one as an open circuit
 198 in the shallow channel (< 30 km depth), and another as a closed circuit in the deeper channel.
 199 The line of flow reversal (dashed white line in Fig. 2B) acts as an internal large-scale shear zone
 200 with curved geometry and thrust motion. The upward flowing layer shows, at shallow depth, a
 201 maximum velocity $\approx 0.5 \times 10^{-9}$ m/s, i.e. ~ 16 mm/year. The line of flow convergence separates
 202 crustal materials of contrasting pressures, one towards the footwall with $P < 1.5$ GPa, the other
 203 towards the hanging wall with $P > 1.5$ GPa (red curve in left hand panel in Fig. 2D), which is the
 204 pressure at which eclogite formation is possible at ~ 30 km. Overall, the flow pattern shows that
 205 significantly overpressured rocks ($TOP > 2.$) can be exhumed rapidly through a narrow region
 206 close to the hanging wall of the channel, which corresponds to the STD in the Himalaya and
 207 where HP and UHP rocks have been found.

208

209 *3.2. Dynamic pressure and overpressure*



Model results are presented as colour maps (Fig. 2) and graphs (Fig. 3), the latter showing the effects of several parameters on overpressure in the subduction channel.

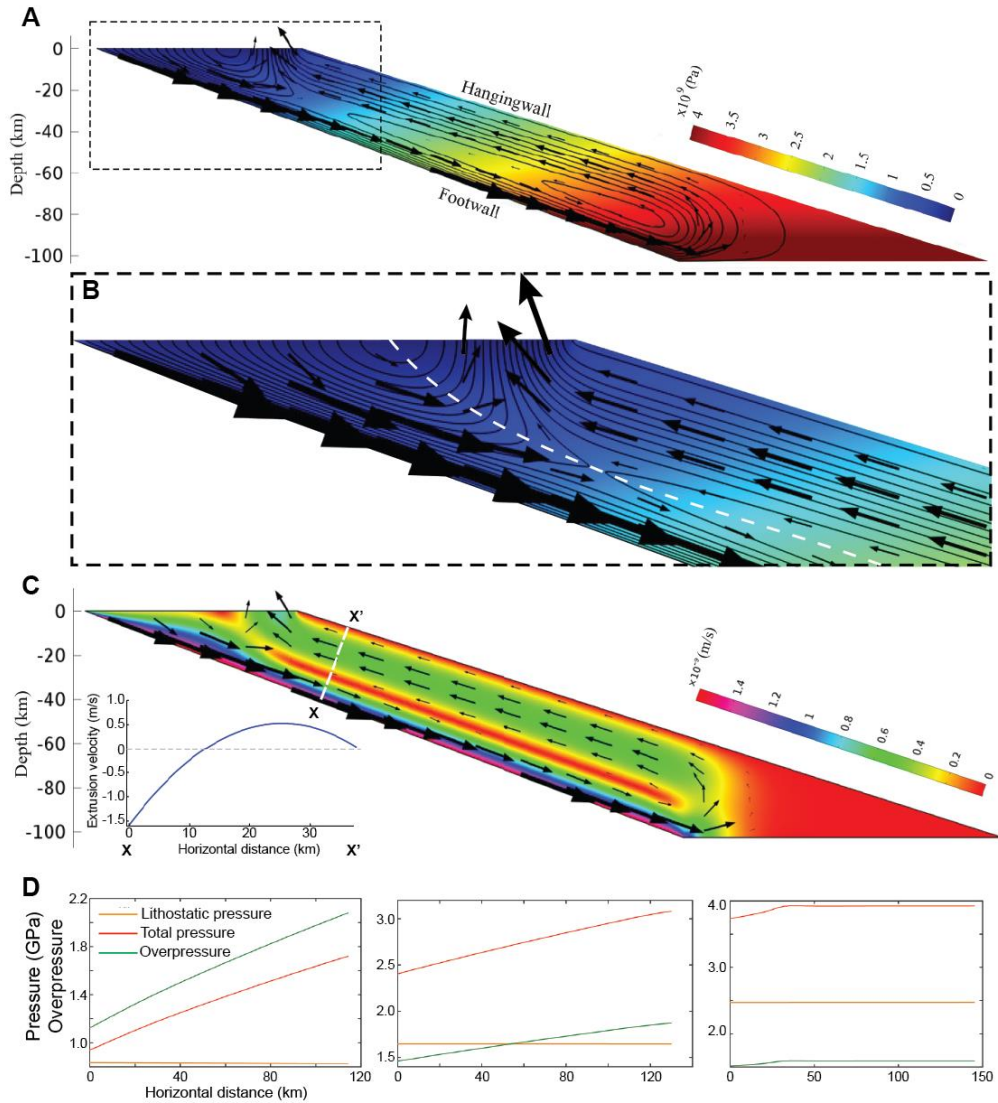


Figure 2. Pressure and velocity maps and graphs for a UTC with $\alpha=20^\circ$, $W_m=100$ km, $W_b=150$ km, $U = 4$ cm/yr, and $\eta = 10^{21}$ Pa s. A – Velocity vectors and streamlines superimposed on pressure map (background colour and colour bar), where two distinct flow circuits can be recognized, one above and the other below -30 km. Also note asymmetry of flow relative to channel, with upward return flow concentrated nearest the hanging wall. B – Zoom of the topmost domain of the channel (marked by dashed rectangle in A). Note the convergence toward the surface between a shallow flow (mostly on the footwall side and carrying lower pressure and overpressure as seen in D) and a deep flow (mostly on the hanging wall side and carrying higher



pressure and overpressure as seen in D). White dashed line separates downward and upward flows. C – Velocity vectors superimposed on velocity coloured map (colour bar for scale). Note the red stripe of lower velocity closer to the footwall, which corresponds to the line of flow reversal in the model. Inset in C showing a velocity profile across the channel (marked by white dashed line and X-X'). D – graphs showing P , PL and $TOP = P/PL$ at -30, -60 and -90 km. Note that the highest overpressure occurs at the shallowest depth, and increases toward the hanging wall (except at -90 km).

Varying W_m with other parameters constant and $\eta = 10^{21}$ Pa s shows that the UTC develops overpressure in the entire range of $W_m/W_b = W_m^* = 25/150$ to $100/150$ km (Fig. 3A). TOP is inversely proportional to W_m^* , and can be as high as 10 for $W_m^* = 0.17$ at depths between 20 and 60 km, with the highest TOP at 20 km depth.

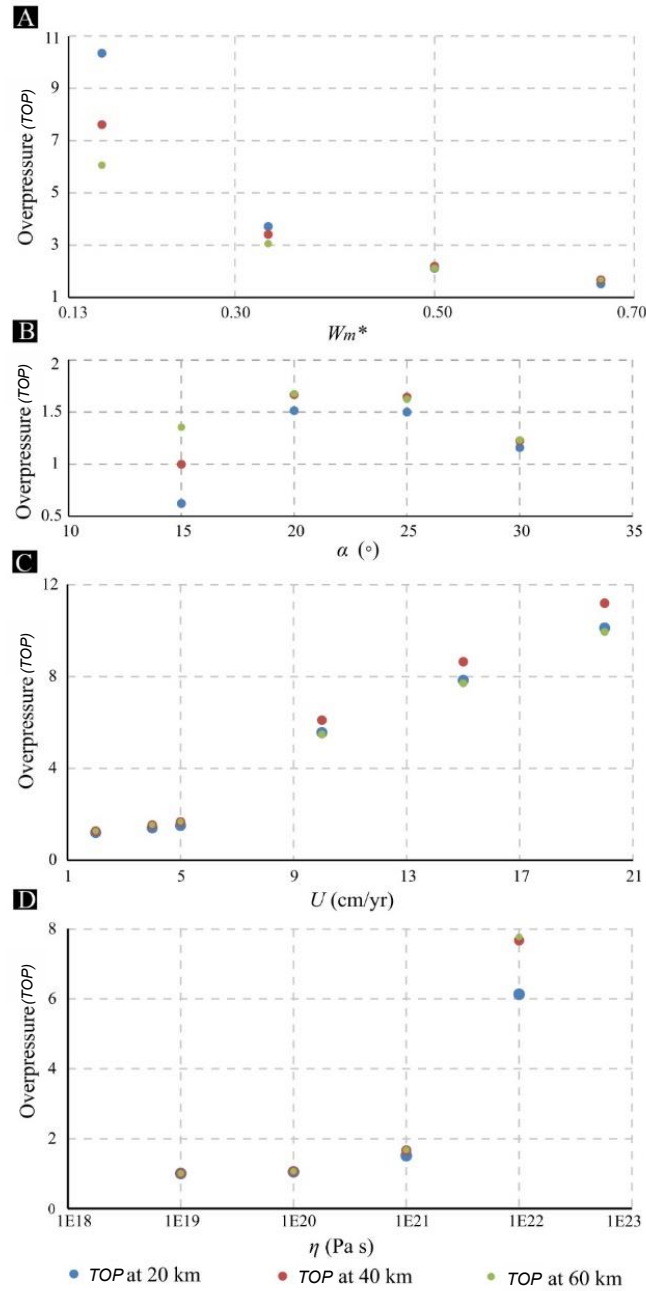
TOP is sensitive to α in a UTC under a given set of values for W_m , η and U (Fig. 3B). The results plotted in Fig. 3B show $TOP > 1$ for $15^\circ < \alpha \leq 30^\circ$. TOP is maximal at $\alpha = 20-25^\circ$, reaching 1.7 at depths between 40 and 60 km.

The plot in Fig. 3C shows increase in TOP with increase in U , from $TOP \approx 1.5$ at $U = 2-5$ cm/yr (current Indian velocity), to $TOP \approx 11$ when $U = 20$ cm/yr (Indian velocity at 60-70 Ma).

The simulations show a near-exponential variation of TOP with η (Fig. 3D), which we use to constrain the viscosity in the Himalayan collision zone.

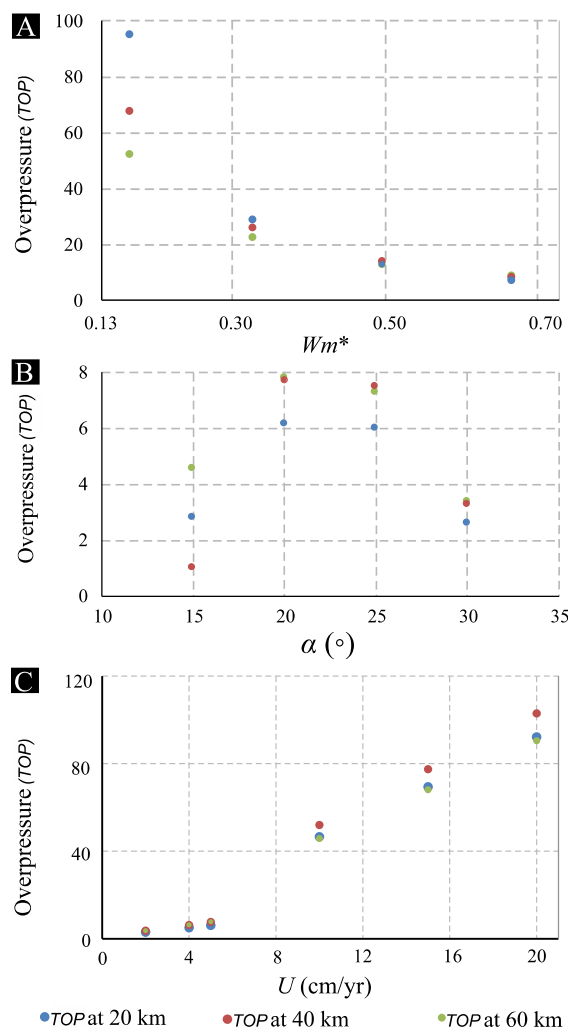
Above we presented numerical simulations for $\eta = 10^{21}$ Pa s, typically applicable to the Himalayan tectonic setting. However, we ran additional simulations with different viscosities, and a set of results is presented for a viscosity of 10^{22} Pa s (Fig. 4). $\eta = 10^{22}$ Pa s induces much higher overpressure, especially when the mouth width decreases, and when the underthrusting velocity increases to velocities that have been estimated to exist at 60-70 Ma.

Taken together, the results shown in Figs. 3 and 4 place constraints on the factors affecting overpressure. Extremely high values of TOP are obtained for $\eta > 10^{21}$ Pa s, $U > 5$ cm/yr, and $W_m^* < 0.50$.



249

250 *Figure 3. Graphs showing the dependence of overpressure factor (TOP) on normalized width of*
 251 *channel mouth W_m^* (A), channel dip α (B), underthrusting velocity U (C), and viscosity in the*
 252 *channel η (D). For each tested variable, other values are kept constant: $W_m^* = 100/150 = 0.67$*
 253 *(except in A), $\alpha = 20^\circ$ (except in B), $U = 5$ cm/a (except in C), $\eta = 10^{21}$ Pa s (except in D).*



254

255 *Figure 4. Graphs showing overpressure factor TOP as a function of normalized channel's mouth*
 256 *width W_m^* (A), channel dip α (B), and convergence velocity U (C), for a viscosity $\eta = 10^{22}$*
 257 *Pa s. For each tested variable, other values are kept constant: $W_m^* = 100/150 = 0.67$ (except*
 258 *in A), $\alpha = 20^\circ$ (except in B), $U = 5$ cm/a (except in C). Comparison with Fig. 3 shows that $\eta =$*
 259 *10^{22} Pa s induces much higher overpressure, especially at smaller W_m^* and higher U .*
 260

261 Varying channel dip (α) involves significant changes in the flow pattern, as shown in Fig.
 262 5. For $\alpha = 15^\circ$, the channel is dominated by downward flow, setting in a large-scale vortex in the
 263 deeper level, and does not show conspicuous zones of ductile extrusion, which only occurs when
 264 $\alpha > 15^\circ$.

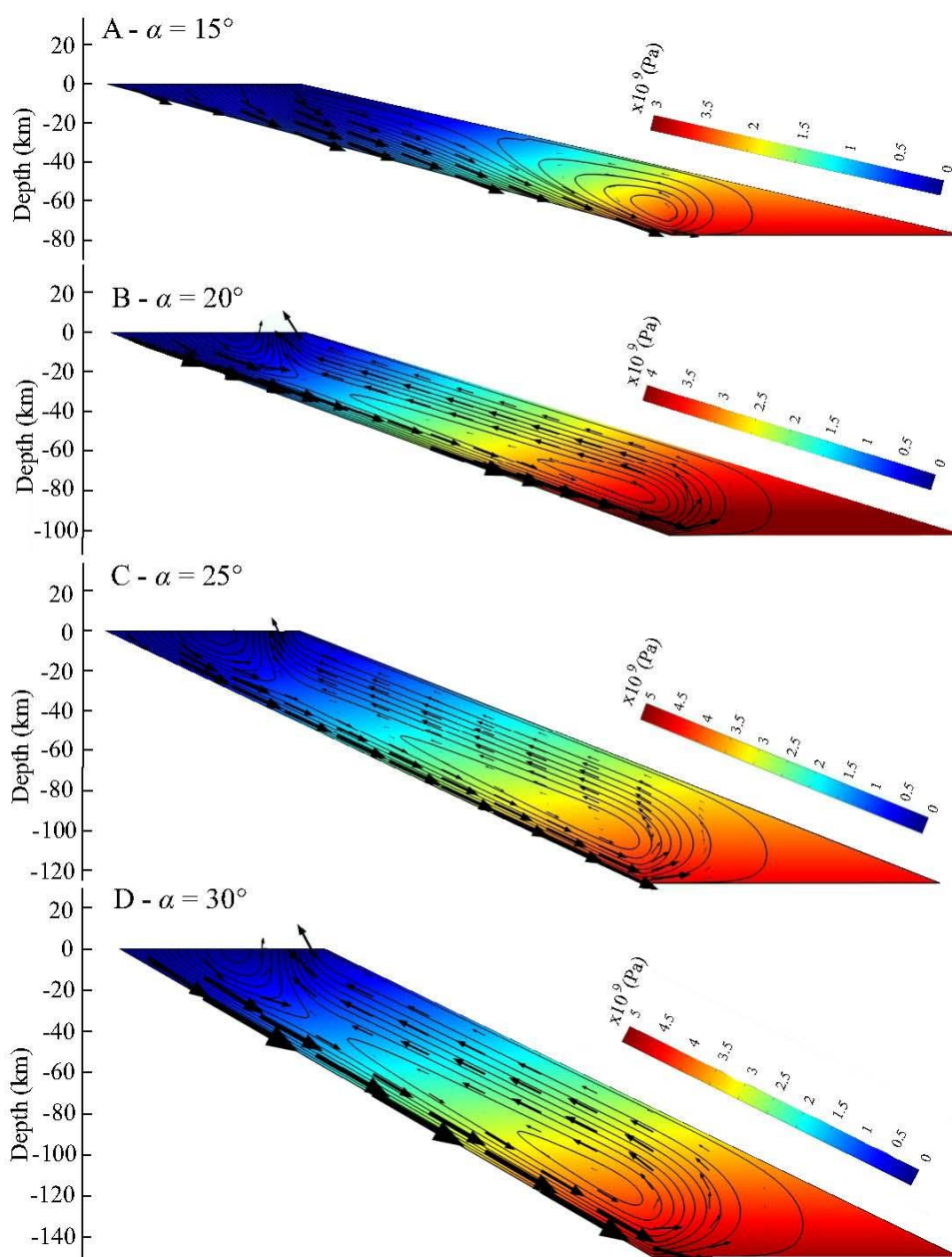


Figure 5. Simulations showing the effects of channel dip (α) on flow pattern.

Besides the results obtained for a channel base width of 150 km, and variable mouth



width, we also evaluated the effects of the channel base width on flow patterns and pressure distribution, by running a set of numerical simulations with a base width of 200 km. The channel flow shows similar patterns in the two cases, and small variations in pressure.

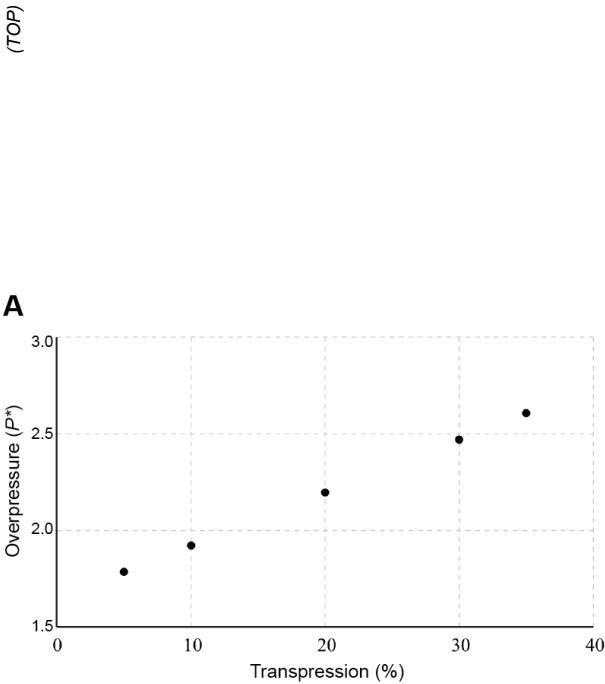


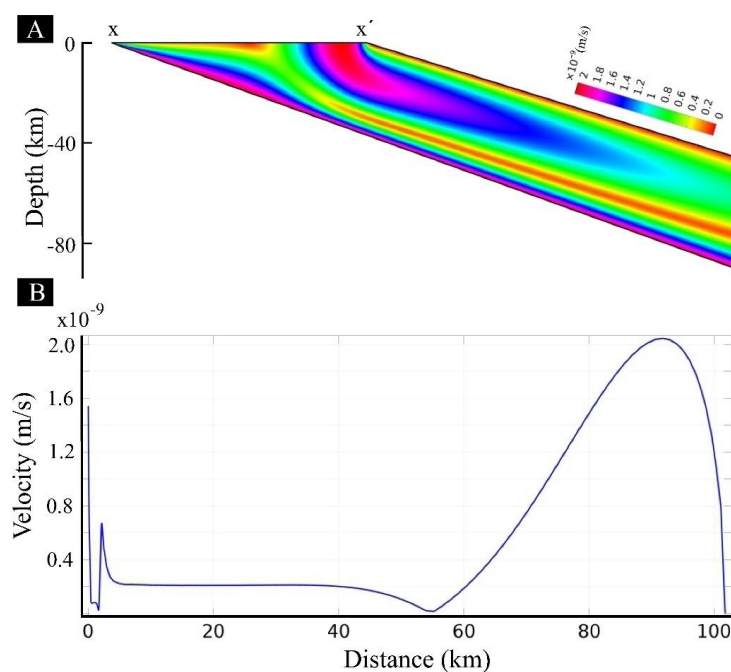
Figure 6. Graphs showing the linear dependence of overpressure (TOP)(A) and extrusion velocity (B) on transpression.

3.3. Effects of transpression on overpressure and flow

We ran a set of simulations to investigate how much a transpressional movement across the viscous channel might influence the magnitude of tectonic overpressure and, especially, velocity at the channels mouth (extrusion velocity). Transpression in the numerical models was introduced by setting the magnitude of horizontal velocity in excess of that corresponding to the



281 underthrusting movement. Fig. 6 shows a plot of TOP as a function of transpression, represented
 282 as the ratio between horizontal velocity and non-transpressional horizontal component (ca.
 283 $1.49\text{E-}9$ m/s). The numerical results indicate that: (1) transpression has appreciable effects on
 284 overpressure, especially if transpression is large ($> 20\%$); (2) transpression has great effects on
 285 extrusion velocity, as shown in Figs. 6 and 7.



286
 287 *Figure 7. A – Velocity map of a channel under transpression. X-X' marks the line along which*
 288 *extrusion velocity was measured and plotted in B.*
 289

290 3.4. Viscous deformable walls

291 We used a similar modelling approach to evaluate the magnitude of overpressure in
 292 subduction channels confined by deformable walls, a model condition that closely replicates the
 293 actual mechanical setting in the Himalayas. This model allows for both channel walls to deform
 294 viscously, thus raising the question of how much overpressure they can retain inside the channel.
 295 We developed the deformable wall models with a channel geometry similar to that in rigid wall



296 models, as shown in Figure 8A. The footwall and the hanging wall of the channel were
297 rheologically modelled as a viscous material, which provides a good approximation for
298 simulation of long term (millions of years) rheology of the lithosphere. Several earlier workers
299 have used viscous rheology to model continental scale deformation during India-Tibet collision.
300 The assumed viscosity values of the cold Indian craton range from 10^{23} to 10^{25} Pa s (e.g.
301 Jiménez-Munt and Platt, 2006; Yang and Liu, 2013), whereas that of Himalayan subducted
302 material ranges between 10^{20} and 10^{21} Pa s (e.g. Liu and Yang, 2003; Copley and McKenzie,
303 2007). The viscosity ratio (viscosity walls/viscosity channel) is therefore in the order of 10^2 to
304 10^5 . In our modelling we chose a conservative value of the viscosity ratio equal to 10^3 , where the
305 walls and channel viscosities are 10^{23} and 10^{20} Pa s, respectively. We constrained the model
306 boundaries with kinematic conditions as in the reference model with rigid walls. The lateral and
307 the top boundaries of the footwall were subjected to a velocity of 4 cm/yr sub-parallel to the
308 channel, whereas the lateral vertical boundaries of the hanging wall were fixed with zero
309 horizontal velocity components, leaving the vertical component unconstrained. Its top boundary
310 was also left unconstrained, allowing the material to extrude upward freely. The wall-channel
311 interfaces had a no-slip condition.

312 Model results show channel flow patterns quite similar to those observed in rigid wall
313 models. The extrusion occurs along a region close to the hanging wall in the form of a Poiseuille
314 flow (Fig. 8A). It is noteworthy that the footwall undergoes little or no deformation, although
315 being deformable. The entire footwall underthrusts by translational motion parallel to the
316 channel. We calculated both the dynamic and the static pressures along the channel axis, and
317 plotted them as a function of depth (Fig. 8B). Similarly to rigid wall models, the dynamic
318 pressure here exceeds the static pressure by nearly 1.5 GPa. For example, the static pressure at a
319 depth of 60 km is about 1.5 GPa, whereas the corresponding dynamic pressure reaches 3 GPa.
320 The pressure plots clearly suggest that subduction channels with deformable walls can also give



rise to large tectonic overpressures. For a viscosity ratio of 10^3 , the deformable wall models are found to be mechanically identical to rigid wall models.

We also used a lower viscosity contrast of 10^2 , and found that even at this relatively low contrast there is significant overpressure in the subduction channel.

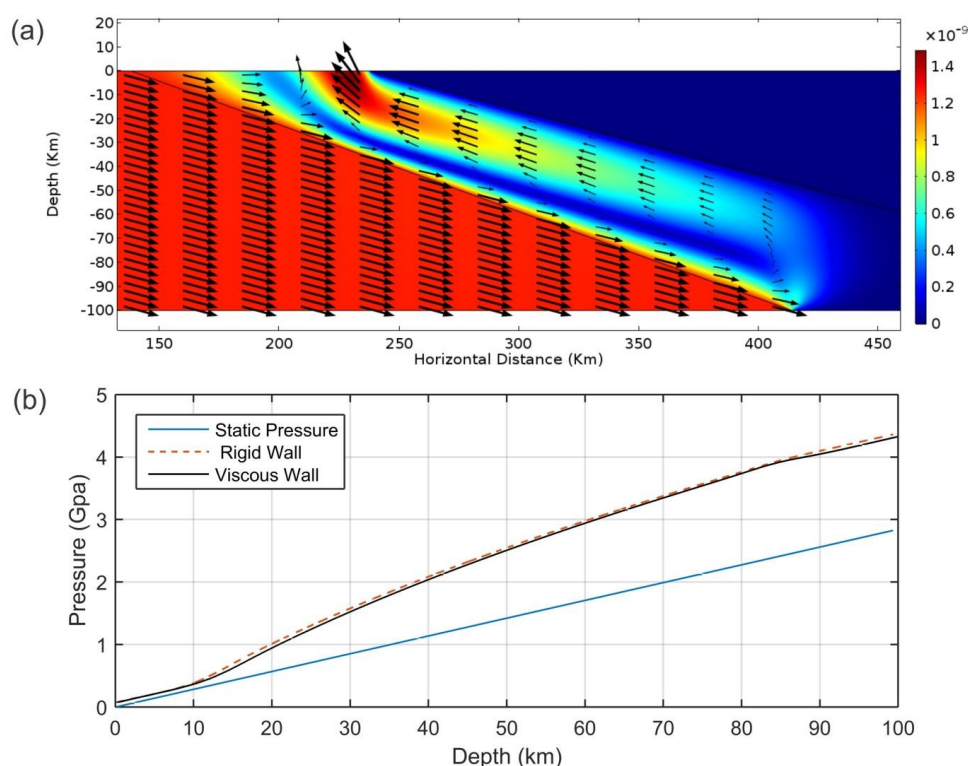


Figure 8. A – Crustal flow patterns in viscous subduction channel and its deformable walls with a viscosity ratio of 10^3 (details of model boundary conditions in the text). B – Calculated plots of pressure as a function of depth along the channel axis. Note that the dynamic pressure obtained from deformable wall models with viscosity contrast 1000 closely follows that for channels with rigid walls.

3.5. Condition at the bottom boundary

This is a critical boundary condition because it is directly related to the retention of overpressure. When we assign an outlet pressure (calculated lithostatic pressure at the depth of the bottom wall) to the bottom wall, TOP does not develop in the whole channel.



337 4. Discussion

338 Given our incomplete knowledge of natural prototypes and the limitations of modelling
339 very complex systems, we have to distinguish between the theoretically and naturally possible
340 values of overpressure. The study here reported for a UTC shows that relevant parameters like
341 channel mouth width (W_m^*), subduction dip (α), underthrusting velocity (U) and viscosity (η)
342 can produce very high overpressure; however, these theoretically possible values have to be
343 constrained by the current knowledge of the Himalayas, in particular exhumation velocities and
344 spatial distribution, occurrence of HP and UHP rocks, and strength of the lithosphere bounding
345 the subduction channel. Despite the natural constraints imposed by our knowledge of the current
346 Himalayas, one cannot ignore that, under specific boundary conditions, geometrical
347 configurations and parameter sets that could have existed in the past (e.g. much higher
348 subduction velocity), high values of overpressure are theoretically possible, which should guide
349 us in the search of new evidence in the natural prototype.

350 Previous models have used two of the three main possible configurations of a subduction
351 channel: parallel-sided and downward tapering, which have been shown to produce relatively
352 small overpressure ($TOP < 3$) (e.g. Li et al., 2010). Here we investigated a different channel
353 geometry, the upward tapering channel. In fact, the parallel-sided geometry corresponds to W_m^*
354 = 1, and can thus be considered an end-member of the UTC. Therefore, we can compare
355 numerical results of overpressure obtained for parallel-sided and UTC channels, by looking at
356 the graph in Fig. 3A where we vary W_m^* . Our best explanation for this effect is that the narrower
357 the mouth the higher the flow confinement, which results in increased velocity gradient in the
358 channel flow, and therefore the dynamic pressure.

359 Previous models can explain channel flow, but neither account for the exhumation of HP
360 rocks (Rubatto et al., 2013), nor the exhumation velocities (Grujic et al., 2011) reported from the
361 Himalayas. Our UTC model provides an alternative explanation for the pressure required for



eclogite metamorphism (Hetényi et al., 2007; Zhang et al., 2014), and the process of rapid exhumation. For exhumation by extrusion to occur in the subduction channel, the flow pattern inside the channel must have a specific configuration, as in the UTC. In such a velocity configuration, underthrusting and exhumation on the channel's footwall add to produce enhanced overthrusting on the MCT, and above the MCT along the line of flow reversal. Conversely, exhumation (upward flow) on the hanging wall is greater than underthrusting and produces relative normal fault displacement on the STD, not because the block to the N of the STD (hanging wall) moves down, but because the rocks south of the STD (footwall) move up due to exhumation by extrusion.

Previous channel flow models can explain the exhumation mechanism, however they leave a number of problems unaddressed. Here we raise some of these issues, pointing to our UTC model as a unifying model to explain the GHS evolution:

- (1) The classical channel flow model assumes that the entire GHS crustal mass thrusts up along the MCT, with concomitant normal motion on the STD (Poiseuille flow). However, recent studies have shown large-scale thrusts within the GHS (Grujic et al., 2011; Larson et al., 2015), suggesting a more complex kinematics of the extrusion process. The UTC model we propose here shows flow partitioning in the channel, leading to thrust-type shear localization within the model GHS.
- (2) A typical channel flow model fails to explain the occurrence of HP rocks (> 1.5 GPa) close to the STD. Our UTC model yields an asymmetrical flow pattern in which HP or UHP materials extrude along a narrow zone located close to the STD.
- (3) The assumption of lithostatic pressure raises two main problems: (i) a conceptual problem, because the subduction channel is dynamic, therefore the lithostatic and dynamic pressures are not identical; and (ii) a practical problem, because the exhumation velocities are calculated on the basis of depth estimated from $\rho g z$ (where z is depth), and not normalized



387 by the overpressure. For instance, conversion of 2 GPa to depth using a static assumption
388 ($\rho g z$) yields a depth of ca. 70 km for a rock density of 2900 kg/m³. However, the UTC flow
389 develops an overpressure in the order of 2 at much smaller depths, and thereby yields lower
390 exhumation rates, as compared to those calculated from petrologic modelling. Estimated
391 metamorphic paths should reflect the shape of the isotherms in the subduction channel,
392 which must have a relationship with velocity in order to carry cold rocks to depth, and
393 preserve the HP and UHP mineral parageneses during exhumation.

394 (4) Model velocities in the channel and at the channel's mouth must be consistent with the values
395 reported in the literature. Assuming lithostatic pressure, an exhumation rate of ~ 15 mm/yr
396 to a depth of at least 15 km was estimated by Ganguly et al. (2000). An estimate of 22–44
397 mm/yr, and increasing linearly with depth was provided by Grujic et al. (2011). According
398 to the UTC dynamic model, the assumption of lithostatic pressure where $TOP = 2$ yields an
399 overestimation of the exhumation velocity by a factor of 2. If this is the case, then the
400 velocity estimates have to be divided by two ($15/2 = 7.5$ mm/yr, and $33/2 = 16.5$ mm/yr).
401 Our UTC model shows a high velocity layer with the materials flowing upward at a rate of
402 16 mm/yr at a depth of ca. 40 km, which is thus in agreement with the estimated average
403 exhumation. The velocity map in Fig. 6 reveals variations of exhumation rates with depth, as
404 predicted for the GHS in the Sikkim Himalaya by Ganguly et al. (2000), who showed that
405 the exhumation was rapid (15 mm/yr) to a depth of 15 km, and then decreased to ca. 2
406 mm/yr until a depth of 5 km. These values estimated for exhumation in the GHS constrain
407 the theoretical values of overpressure numerically obtained by varying the amount of
408 transpression. Transpression values > 10% imply velocities at the mouth (exhumation) much
409 larger than estimated for the GHS, therefore we conclude that transpression must be very
410 limited (< 10%).

411 (5) A critical issue regarding overpressure in a subduction channel is the strength of the channel



walls to support high overpressure values. The most debatable point in our modelling is the use of rigid walls. For this discussion, we can compare the subduction channel to a pressure vessel, in which the resistance of the vessel to internal pressure depends on two main parameters: the strength of the vessel (the lithosphere hosting the subduction zone), and the thickness of the pressure vessel walls (hoop stress). In nature, if the walls of the pressure vessel (subducting and overlying lithospheres) are old and cold, which is the case in the Himalayan collision, then their mechanical strength can be very high. If, additionally, the cold and strong lithosphere is thick, then the walls of the subduction channel can support high overpressure, as indicated by the numerical results with viscous deformable walls. Given that the Indian plate and the TSS above the STD are almost undeformed (attesting to the rigidity contrast between foot and hanging walls of the GHS) and thick, the channel walls were assumed undeformable in the reference simulations. In order to investigate the effects of viscous deformable walls on tectonic overpressure, we used viscosity contrasts (viscosity of channel walls/viscosity of subduction channel) down to 100, which are well within the accepted values of lithosphere viscosity (up to 10^{23} Pa s) and subducted material (down to 10^{19} Pa s). These simulations indicate that viscosity contrasts of 1000 or 100 do not change significantly the overpressure obtained with rigid walls. Another critical issue in overpressure build-up is the condition at the bottom boundary: if an outlet pressure is assigned to the bottom wall, then this boundary behaves as a leaking boundary that cannot retain dynamic pressure. However, the cold, thick and strong lithospheres that comprise the Indian and Eurasian plates are a good argument against a leaking bottom boundary in a flat-ramp geometry such as the Himalayan collision zone.

(6) In order to explain the non-linear variation of overpressure with channel dip (α) we need to analyse the variations of channel flow patterns with increasing α (Fig. 5). For low α values (15°), the underthrusting motion drags materials to a larger extent into the downward flow,



437 and produces a large vortex in the deeper channel, where the curl dominates the flow field.
438 Consequently, the dynamic pressure remains low. Note that flow divergence increases the
439 dynamic pressure. With increasing α (20°) the flow pattern is characterized by the
440 development of an extrusion channel on the hanging wall side, along which the material
441 extrudes upward with flow convergence at the mouth. Such a negative divergence in the
442 flow builds overpressure on the hanging wall side (Fig. 2D). With further increase in α the
443 extrusion channel widens, and causes the overpressure to drop, as it happens in a pipe flow.
444 This is the reason why the overpressure has a maximum at α around 20 - 25° .

445 (7) Inverted metamorphic grade has not been explained by previous models, but the UTC can
446 provide an explanation if one considers the flow pattern shown in Fig. 2B. HP and UHP
447 rocks can be exhumed by two flow cells, both inverting metamorphism because low-grade
448 rocks go down close to the footwall, and high-grade rocks are exhumed close to the hanging
449 wall.

450

451 We analysed the consistency between the numerical results and geological/geophysical
452 data to constrain the most probable viscosity and pressure, at the same time satisfying a
453 reasonable velocity at the channel's mouth (i.e. exhumation rates) (Fig. 7). On the one hand, the
454 viscosity of rocks comprising the lithosphere can vary between 10^{19} and 10^{23} Pa s. On the other
455 hand, overpressure is sensitive to the viscosity within the UTC, increasing exponentially with
456 increase in viscosity. Additionally, from the values shown in Figs. 3 and 4, the formation of HP
457 rocks can occur at very shallow levels if $\eta = 10^{21}$ Pa s. However, despite the relatively wide
458 range of possible viscosity values, $\eta > 10^{21}$ Pa s in a Himalayan UTC yields overpressures > 8 .
459 This means that, for $\eta = 10^{22}$ Pa s, a rock metamorphosed at 50 km depth would record a total
460 pressure equivalent to the lithostatic pressure at a depth of 400 km, which is not acceptable on
461 the basis of our current knowledge of subduction zone dynamics. Therefore, we propose that the



viscosity in the subduction channel is probably in the range $10^{20} \leq \eta \leq 10^{21}$ Pa s.

Regarding the discrepancy between previous estimates of possible values of overpressure and ours, we call attention to two factors: (1) we use a subduction channel geometry, the UTC, not investigated previously; and (2) the values reported here are very large only for small W_m^* , or $U > 5$ cm/a, or $\eta > 10^{21}$ Pa s. In other words, for relatively small tapering (W_m^*), average plate tectonics velocities, and reasonable viscosities, the numerical results reported here for overpressure are not excessive, but nevertheless still very important as a factor for depth overestimation. The values used for the controlling parameters, W_m^* , α and η are conservative; in fact, the model channel in Fig. 1C shows rather small tapering as compared with the cross-section in Fig. 1B, but, nevertheless, the model overpressure is still quite high, especially at low depth.

The UTC simulations show that there is no need for gravitational collapse, buoyancy-controlled crustal exhumation, or orogen-perpendicular pressure gradient induced by a topographic gradient to explain simultaneous reverse and normal fault kinematics on MCT and STD, or inverse metamorphic grade, or exhumation of HP rocks. We conclude that flow in a UTC, without the need for topography or density contrasts, can be responsible for these three simultaneous and seemingly paradoxical processes in the Himalayas.

The formation and exhumation of high (HP) and ultra-high (UHP) pressure rocks is a persisting fundamental problem, especially regarding UHP rocks. The problem is even greater if one assumes that pressure estimated from paleopiezometry can be converted directly to depth, because then the UHP rocks must be exhumed from great depths. Several models have been proposed for the exhumation of HP and UHP rocks in several orogens (e.g. Hacker and Gerya, 2013; Warren, 2013; Burov et al., 2014a, 2014b): channel flow (e.g. England and Holland, 1979; Mancktelow, 1995; Grujic et al., 1996; Beaumont et al., 2001, 2009; Burov et al., 2001; Raimbourg et al., 2007; Gerya et al., 2008; Warren et al., 2008; Li and Gerya, 2009); eduction



(e.g. Andersen et al., 1991; Kylander-Clark et al., 2012); buoyancy-driven crustal delamination and stacking (e.g. Chemenda et al., 1995, 1996; Sizova et al., 2012); microplate rotation (e.g. Hacker et al., 2000; Webb et al., 2008); trans-mantle diapirism (e.g. Stöckhert and Gerya, 2005; Little et al., 2011; Gordon et al., 2012); and slab rollback (e.g. Brun and Faccenna, 2008; Faccenda et al., 2009; Vogt and Gerya, 2014; Malusà et al., 2015). No model has so far provided a complete and unique explanation. The UTC model presented here is a potentially unifying model, because it shows that it is possible to form rocks recording HP or UHP at depths < 60 km and to exhume them to the surface as a consequence of the flow configuration in the UTC.

495

5. Conclusion

The UTC model integrates and provides a robust physical explanation for a number of landmark features in the Greater Himalayan geodynamics, such as simultaneous reverse and normal faulting (channel flow), inversion of the metamorphic grade in the GHS, and exhumation of HP/UHP rocks along a narrow conduit close to the STD. Viscous flow in a UTC involves dynamic pressures in excess of lithostatic pressure, resulting in significant overpressure by a factor more than 1.5, even at depths as shallow as 40 km. The UTC model predicts high pressure (>1.5 GPa) metamorphism of underthrust rocks, e.g. eclogitization, to occur above 60 km depth. The UTC model shows that the GHS is segmented broadly into two sub-terrains with contrasting pressures: wide southern and narrow northern terranes, with pressures less and greater than 1.5 GPa, respectively. It further shows that temporal variations in channel dip may promote ($\alpha > 15^\circ$) or inhibit ($\alpha < 15^\circ$) exhumation. Overpressure increases with increase in U , from $TOP \approx 1.5$ for $U = 2-5$ cm/yr (current Indian velocity), to $TOP \approx 11$ when $U = 20$ cm/yr (Indian velocity at 60-70 Ma), which means that in the past all the dynamic processes discussed here may have been enhanced. We tested different model setups (e.g. parallel walls) and boundary conditions (e.g. slip or no-slip condition at bounding walls), but these do not reproduce



512 the prototype. The UTC model shows that tectonic pressure alone can drive the extrusion of HP
513 rocks by channel flow. Viscous deformable walls do not affect overpressure significantly for
514 viscosity contrasts (viscosity walls/viscosity channel) in the order of 1000 or 100. If, during the
515 subduction process, the mouth width, or the dip, or the velocity, or the viscosity, or the
516 conditions at the boundaries change in space and time, then *TOP* will change accordingly, and
517 the exhumation mechanism (flow in the channel) and exhumation depth will also change.

518 *TOP* in a UTC is only possible if the condition at the bottom boundary is not outlet
519 pressure; otherwise it behaves as a leaking boundary that cannot retain dynamic pressure.
520 However, the cold, thick and strong lithospheres that comprise the Indian and Eurasian plates are
521 a good argument against a leaking bottom boundary in a flat-ramp geometry, which means that
522 overpressure can build up to high values in the GHS. The argument does not apply if the channel
523 is “open” at the bottom, because overpressure cannot be retained. This could be the case in
524 subduction zones where there is no evidence for return flow and exhumation concomitant with
525 subduction.

526 The numerical results reported here show that, under specific boundary conditions,
527 geometrical configurations, and parameter sets, high values of overpressure are theoretically
528 possible, which should guide us in the search of new evidence in the natural prototype to prove
529 or disprove the natural existence of high overpressure.

530

531 **Acknowledgements**

532 FOM benefited from a sabbatical fellowship awarded by FCT Portugal
533 (SFRH/BSAB/1405/2014). NM acknowledges DST-SRB, India, for providing a J.C. Bose
534 Fellowship. SG acknowledges funding for doctoral research from the University Grants
535 Commission (UGC/275/Jr Fellow (Sc.)). GR thanks Carleton University for research support.

536



537 **References**

- 538 Andersen, T.B., Jamtveit, B., Dewey, J.F., Swensson, E., 1991. Subduction and eduction of
539 continental crust: major mechanism during continent–continent collision and orogenic
540 extensional collapse, a model based on the south Caledonides. *Terra Nova* 3, 303–310.
- 541 Beaumont, C., Jamieson, R.A., Butler, J.P., Warren, C.J., 2009. Crustal structure: a key
542 constraint on the mechanism of ultra-high-pressure rock exhumation. *Earth and Planetary
543 Science Letters* 287, 116–129.
- 544 Beaumont, C., Jamieson, R. A., Nguyen, M. H., Lee, B., 2001. Himalayan tectonics explained by
545 extrusion of a low-viscosity crustal channel coupled to focused surface denudation. *Nature*
546 414, 738–742.
- 547 Brun, J.-P., Faccenna, C., 2008. Exhumation of high-pressure rocks driven by slab rollback.
548 *Earth and Planetary Science Letters* 272, 1–7.
- 549 Burov, E., Jolivet, L., Le Pourhiet, L., Poliakov, A., 2001. A thermomechanical model of
550 exhumation of high pressure (HP) and ultra-high pressure (UHP) metamorphic rocks in
551 Alpine-type collision belts. *Tectonophysics* 342, 113–136.
- 552 Burov, E. et al, 2014a. Rheological and geodynamic controls on the mechanisms of subduction
553 and HP/UHP exhumation of crustal rocks during continental collision: Insights from
554 numerical models. *Tectonophysics* 631, 212–250.
- 555 Burov, E., François, T., Yamato, P., Wolf, S., 2014b. Mechanisms of continental subduction and
556 exhumation of HP and UHP rocks. *Gondwana Research* 25, 464–493.
- 557 Chemenda, A.I., Mattauer, M., Malavieille, J., Bokun, A.N., 1995. A mechanism for syn-
558 collisional rock exhumation and associated faulting: Results from physical modelling. *Earth
559 Planet. Sci. Lett.* 132, 225–232.
- 560 Chemenda, A.I., Mattauer, M., Bokun, A.N., 1996. Continental subduction and a mechanism for
561 exhumation of high-pressure metamorphic rocks: new modeling and field data from Oman.
562 *Earth and Planetary Science Letters* 143, 173–182.
- 563 Copley, A. & McKenzie, D. 2007. Models of crustal flow in the India-Asia collision zone.
564 *Geophysical Journal International*, 169, 683–698.
- 565 Copley, A., Avouac, J. P., Wernicke, B. P., 2011. Evidence for mechanical coupling and strong
566 Indian lower crust beneath southern Tibet. *Nature* 472, 79–81.
- 567 Corrie, S.L., Kohn, M.J., Vervoort, J.D., 2010. Young eclogite from the Greater Himalayan
568 Sequence, Arun Valley, eastern Nepal: P–T–t path and tectonic implications. *Earth Planet.
569 Sci. Lett.* 289, 406–416.



- 570 DeMets, C., Gordon, R. G., Argus, D. F., 2010. Geologically current plate motions. *Geophys. J.*
571 *Int.* 181, 1–80.
- 572 England, P.C., Holland, T.J.B., 1979. Archimedes and the Tauern eclogites: the role of buoyancy
573 in the preservation of exotic eclogite blocks. *Earth and Planetary Science Letters* 44, 287–
574 294.
- 575 England, P. C., Houseman, G. A., 1989. Extension during continental convergence, with
576 application to the Tibetan Plateau. *J. Geophys. Res.* 94, 17,561–17,579.
- 577 Faccenda, M., Minelli, G., Gerya, T.V., 2009. Coupled and decoupled regimes of continental
578 collision: numerical modeling. *Earth and Planetary Science Letters* 278, 337–349.
- 579 Feldl, N., Bilham, R., 2006. Great Himalayan earthquakes and the Tibetan plateau. *Nature* 444,
580 165–170.
- 581 Ganguly, J., Dasgupta, S., Cheng, W. J., Neogi, S., 2000. Exhumation history of a section of the
582 Sikkim Himalayas, India: records in the metamorphic mineral equilibria and compositional
583 zoning of garnet. *Earth Planet. Sci. Lett.* 183, 471–486.
- 584 Gansser, A., 1964. *Geology of the Himalayas*. Wiley-Interscience, New York, pp. 289.
- 585 Gerya, T.V., Perchuk, L.L., Burg, J.-P., 2008. Transient hot channels: perpetrating and
586 regurgitating ultrahigh-pressure, high temperature crust–mantle associations in collision
587 belts. *Lithos* 103, 236–256.
- 588 Gordon, S.M. et al., 2012. Multi-stage exhumation of young UHP-HP rocks: timescales of melt
589 crystallization in the D'Entrecasteaux Islands, southeastern Papua New Guinea. *Earth and*
590 *Planetary Science Letters* 351–352, 237–246.
- 591 Groppo, C., Lombardo, B., Rolfo, F., Pertusati, P., 2007. Clockwise exhumation path of
592 granulitized eclogites from the Ama Drime range (Eastern Himalayas). *J. Metamorph. Geol.*
593 25, 51–75.
- 594 Grujic, D. et al., 1996. Ductile extrusion of the Higher Himalayan Crystalline in Bhutan:
595 evidence from quartz microfabrics. *Tectonophysics* 260, 21–43.
- 596 Grujic, D., Warren, C. J., Wooden, J. L., 2011. Rapid synconvergent exhumation of Miocene-
597 aged lower orogenic crust in the eastern Himalaya. *Lithosphere* 3, 346–366.
- 598 Hacker, B.R. et al., 2000. Exhumation of ultrahigh-pressure continental crust in east– central
599 China: Late Triassic–Early Jurassic tectonic unroofing. *Journal of Geophysical Research*
600 105, 13339–13364.
- 601 Hacker, B.R., Gerya, T.V., 2013. Paradigms, new and old, for ultrahigh-pressure tectonism.
602 *Tectonophysics* 603, 79–88.
- 603 Hetényi, G. et al., 2007. Density distribution of the India plate beneath the Tibetan plateau:



- 604 geophysical and petrological constraints on the kinetics of lower-crustal eclogitization. *Earth*
605 *Planet. Sci. Lett.* 264, 226–244.
- 606 Kellett, D. A., Grujic, D., Coutand, I., Cottle, J., Mukul, M., 2013. The South Tibetan
607 detachment system facilitates ultra rapid cooling of granulite-facies rocks in Sikkim
608 Himalaya. *Tectonics* 32, 252–270.
- 609 Kylander-Clark, A., Hacker, B., Mattinson, C., 2012. Size and exhumation rate of ultrahigh-
610 pressure terranes linked to orogenic stage. *Earth and Planetary Science Letters* 321–322,
611 115–120.
- 612 Jiménez-Munt, I., Platt, J. P., 2006. Influence of mantle dynamics on the topographic evolution of
613 the Tibetan Plateau: Results from numerical modeling. *Tectonics*, vol. 25, TC6002,
614 doi:10.1029/2006TC001963
- 615 Larson, K. P., Ambrose, T. K., Webb, A. G., Cottle, J. M., Shrestha, S., 2015. Reconciling
616 Himalayan midcrustal discontinuities: The Main Central thrust system. *Earth Planet. Sci.*
617 *Lett.* 429, 139–146.
- 618 Li, Z., Gerya, T. V., 2009. Polyphase formation and exhumation of high- to ultrahigh pressure
619 rocks in continental subduction zone; numerical modeling and application to the Sulu
620 ultrahigh-pressure terrane in eastern China. *Journal of Geophysical Research* 114 (B9).
- 621 Little, T. A. et al., 2011. Diapiric exhumation of Earth's youngest (UHP) eclogites in the gneiss
622 domes of the D'Entrecasteaux Islands, Papua New Guinea. *Tectonophysics* 510, 39–68.
- 623 Liu, M., Yang, Y., 2003. Extensional collapse of the Tibetan Plateau: results of three-
624 dimensional finite element modeling. *Journal of Geophysical Research* 108,
625 2361. <http://dx.doi.org/10.1029/2002JB002248>
- 626 Malusà, M. G. et al., 2015. Contrasting styles of (U)HP rock exhumation along the Cenozoic
627 Adria-Europe plate boundary (Western Alps, Calabria, Corsica). *Geochemistry Geophysics*
628 *Geosystems* 16, 1786–1824.
- 629 Mancktelow, N., 1995. Nonlithostatic pressure during sediment subduction and the development
630 and exhumation of high pressure metamorphic rocks. *J. Geophys. Res.* 100, 571–583.
- 631 Marques, F. O., Ranalli, G., Mandal, N., 2018. Tectonic overpressure at shallow depth in the
632 lithosphere: The effects of boundary conditions. *Tectonophysics*, in press.
- 633 Nábělek, J. et al., 2009. Underplating in the Himalaya-Tibet collision zone revealed by the Hi-
634 CLIMB experiment. *Science* 325, 1371–1374.
- 635 O'Brien, P. J., Zotov, N., Law, R., Khan, M. A., Jan, M. Q., 2001. Coesite in Himalayan eclogite
636 and implications for models of India-Asia collision. *Geology* 29, 435–38.
- 637 Raimbourg, H., Jolivet, L., Leroy, Y., 2007. Consequences of progressive eclogitization on



- 638 crustal exhumation, a mechanical study. *Geophysical Journal International* 168, 379–401.
- 639 Rubatto, D., Chakraborty, S., Dasgupta, S., 2013. Timescales of crustal melting in the Higher
- 640 Himalayan Crystallines (Sikkim, Eastern Himalaya) inferred from trace element-constrained
- 641 monazite and zircon chronology. *Contrib. Mineral. Petrol.* 165, 349–372.
- 642 Schulte-Pelkum, V. et al., 2005. Imaging the Indian subcontinent beneath the Himalaya.
- 643 *Nature* 435, 1222–1225.
- 644 Sizova, E., Gerya, T.V., Brown, M., 2012. Exhumation mechanisms of melt-bearing ultrahigh
- 645 pressure crustal rocks during collision of spontaneously moving plates. *Journal of*
- 646 *Metamorphic Geology* 30, 927–955.
- 647 Sorcar, N., Hoppe, U., Dasgupta, S., Chakraborty, S., 2014. High-temperature cooling histories
- 648 of migmatites from the High Himalayan Crystallines in Sikkim, India: rapid cooling
- 649 unrelated to exhumation? *Contrib. Mineral. Petrol.* 167, 957.
- 650 Stöckhert, B., Gerya, T.V., 2005. Pre-collisional high pressure metamorphism and nappe
- 651 tectonics at active continental margins: a numerical simulation. *Terra Nova* 17, 102–110.
- 652 Vogt, K., Gerya, T.V., 2014. From oceanic plateaus to allochthonous terranes: numerical
- 653 modelling. *Gondwana Research* 25, 494–508.
- 654 Unsworth, M.J. et al., 2005. Crustal rheology of the Himalaya and Southern Tibet inferred from
- 655 magnetotelluric data. *Nature* 438, 78–81.
- 656 Warren, C.J., 2013. Exhumation of (ultra-)high-pressure terranes: concepts and mechanisms.
- 657 *Solid Earth* 4, 75–92.
- 658 Warren, C.J., Beaumont, C., Jamieson, R.A., 2008. Modelling tectonic styles and ultra-high
- 659 pressure (UHP) rock exhumation during the transition from oceanic subduction to continental
- 660 collision. *Earth and Planetary Science Letters* 267, 129–145.
- 661 Warren, C.J., Grujic, D., Kellett, D. A., Cottle, J., Jamieson, R. A., Ghalley, K. S., 2011. Probing
- 662 the depths of the India–Asia collision: U–Th–Pb monazite chronology of granulites from
- 663 NW Bhutan. *Tectonics* 30, TC2004.
- 664 Webb, L.E., Baldwin, S.L., Little, T.A., Fitzgerald, P.G., 2008. Can microplate rotation drive
- 665 subduction inversion? *Geology* 36, 823–826.
- 666 Wobus, C. et al., 2005. Active out-of-sequence thrust faulting in the central Nepalese Himalaya.
- 667 *Nature* 434, 1008–1011.
- 668 Yang, Y., Liu, M., The Indo-Asian continental collision: A 3-D viscous model, *Tectonophysics*
- 669 (2013), <http://dx.doi.org/10.1016/j.tecto.2013.06.032>
- 670 Zhang, Z. et al., 2015. Oligocene HP metamorphism and anatexis of the Higher Himalayan
- 671 Crystalline Sequence in Yadong region, east-central Himalaya. *Gondwana Research*,



672 doi:10.1016/j.gr.2015.03.002.
673 Zhang, Z. et al., 2014. The Moho beneath western Tibet: Shear zones and eclogitization in the
674 lower crust. Earth Planet. Sci. Lett. 408, 370-377.
675
676



677 **Appendix - Methods**

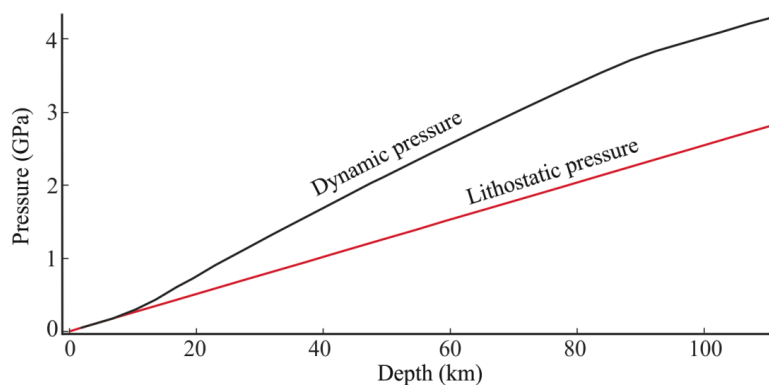
678 *Boundary conditions and model setup*

679 The boundary conditions needed to complete the mathematical formulation for numerical
 680 simulations were as follows: (1) slab-parallel velocity applied on the underthrusting wall,
 681 consistent with the horizontal velocity of the Indian plate (5 cm/yr, DeMets et al., 2010); (2) slip
 682 condition on (parallel to) the bottom boundary (Nábělek et al., 2009); (3) no slip condition on the
 683 hanging wall; (4) outlet condition with 1 atm pressure at the channel's mouth; (5) gravity applied
 684 to the whole channel ($\sim 9.8 \text{ m/s}^2$); (6) constant density of the material in the channel = 2800
 685 kg/m^3 (no phase changes in the models), representing the association felsic (mostly) and mafic
 686 granulites carrying the eclogite pods. Given that the Indian plate and the TSS above the STD are
 687 almost undeformed, attesting to the rigidity contrast between foot and hanging walls of the GHS,
 688 the channel walls were assumed undeformable in the simulations, except those testing the effects
 689 of viscous walls. In order to investigate flow kinematics and dynamic pressure in the channel, we
 690 varied the following parameters: (1) channel viscosity (η), (2) underthrusting velocity (U), (3)
 691 channel dip (α), (4) channel mouth's width (W_m), and (5) viscosity of channel walls. The
 692 viscosity in the channel was varied between 10^{19} and 10^{22} Pa s to cover a broad spectrum of
 693 crustal viscosities, as reported in the literature (Beaumont et al., 2001; England and Houseman,
 694 1989; Copley et al., 2011). The current convergence rate between India and Eurasia has been
 695 estimated in the order of 5 cm/yr, however, given the wide range of estimated velocities (Feldl
 696 and Bilham, 2006; DeMets et al., 2010), we ran numerical simulations varying U between 2 and
 697 20 cm/yr ($6.34\text{E-}10$ to $6.34\text{E-}9$ m/s in the model). Channel dip was varied between 15 and 30°,
 698 which broadly covers the geometry of the GHS shown in different geological sections. We
 699 assumed $W_m = 25$ to 100 km, and W_b (width at the channel's base) = 150 or 200 km, from which
 700 we define $W_m^* = W_m/W_b$. We tested a viscosity contrast (viscosity of channel walls/viscosity in
 701 the channel) of 1000 to investigate the effects of viscous deformable walls on overpressure.



702 Despite varying all these parameters, the prime focus of our investigation concerned the
703 simulations with $U = 5$ cm/yr, $\alpha = 20^\circ$, $W_m = 100$ km and $W_b = 150$ km, as they represent the
704 most common and conservative values regarding published data. We then use the numerical
705 results to constrain the viscosity, pressure and velocity in the channel, consistent with current
706 geological data and estimates.

707 The metamorphic processes occur in response to the total isotropic stress, called *dynamic*
708 *pressure*, which is a sum of the tectonic (Stokes) and lithostatic pressures ($\rho g z$, where ρ is
709 density, g is gravitational acceleration, and z is depth) (Figs. A1 and A2). The dynamic pressure
710 results from the viscous flow driven by tectonic stresses in the gravity field. Using the present
711 mechanical model, we evaluate the dynamic pressure to explain the occurrence of high-pressure
712 rocks in the GHS, as a consequence of dynamic pressure in excess of lithostatic pressure at a
713 given crustal depth. We define an overpressure factor (*TOP*) as the non-dimensional ratio
714 between dynamic and lithostatic pressures. For a better understanding of overpressure in a UTC,
715 we carried out a parametric study of *TOP* as a function of η , W_m , α , U , and effective
716 convergence velocity (horizontal velocity component $> U$).



717
718 *Figure A1. Evolution of dynamic and lithostatic pressures in a UTC with $\eta = 10^{21}$ Pa s and $\rho =$*
719 *2800 kg/m³. The ratio dynamic pressure/lithostatic pressure corresponds to the overpressure*
720 *factor (TOP).*

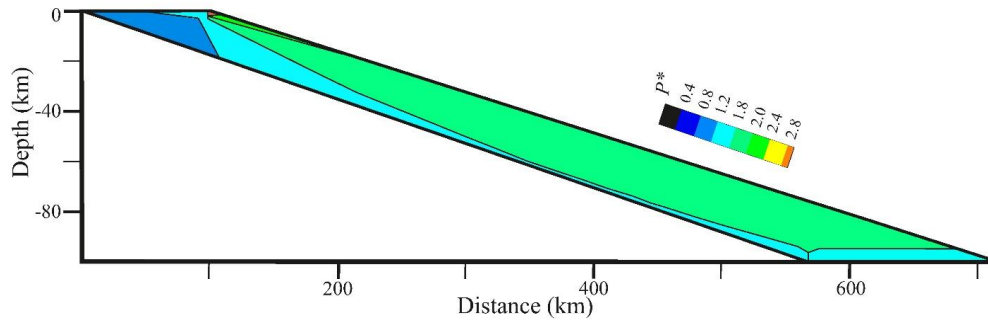


Figure A2. Overpressure in the UTC under the velocity field shown in Fig. 3.

Mathematical formulation

The mathematical model used in the present work is based on the Navier-Stokes equations for two-dimensional steady-state incompressible viscous flows:

$$\rho \left(\frac{\partial \mathbf{u}}{\partial t} + \mathbf{u} \cdot \nabla \mathbf{u} \right) = -\nabla p + \eta \nabla^2 \mathbf{u} + \mathbf{F} \quad (1)$$

$$\nabla \cdot \mathbf{u} = 0 \quad (2)$$

where \mathbf{u} is the velocity vector, p the pressure, ρ the density, η the dynamic viscosity and \mathbf{F} the external body force (gravity). ρ and η are constant. Then, defining the scaled variables $\bar{x} = x/L$, $\bar{u} = u/U$, $\bar{p} = p/P$ and $\bar{t} = t/T$, in terms of the characteristic length L , velocity U , pressure P and time $T = L/U$, Eqs. (1) and (2) become:

$$\frac{\partial \bar{\mathbf{u}}}{\partial \bar{t}} + \bar{\mathbf{u}} \cdot \nabla \bar{\mathbf{u}} = -\text{Eu} \bar{\nabla} \bar{p} + \frac{1}{\text{Re}} \bar{\nabla}^2 \bar{\mathbf{u}} \quad (3)$$

$$\bar{\nabla} \cdot \bar{\mathbf{u}} = 0 \quad (4)$$

where $\text{Re} = \rho UL/\eta$ and $\text{Eu} = P/\rho U^2$ are, respectively, the Reynolds and Euler numbers. For flows at low characteristic velocity U and high viscosity η , inertial terms Eu and Re in Eq. (3) become negligible. We thus obtain the Stokes approximation of the momentum equation for quasi-static



(creeping) flows, which in dimensional form and under a gravity field reads:

$$-\nabla p + \eta \nabla^2 \mathbf{u} + \mathbf{F} = 0 \quad (5)$$

The Stokes equations were solved on the 2-D domain illustrated in Fig. 1C, which was

filled with an incompressible viscous linear fluid. The flow equations, with the boundary

conditions specified, were solved in the primitive variables $\mathbf{u} \equiv (u, v)$ and p over a finite element

mesh, using the algorithm for incompressible Stokes flows implemented in COMSOL.